Available online at www.sciencedirect.com
SCIENCE DIRECT®
ELSEVIER
Nuclear Instruments and Methods in Physics Research A 524 (2004) 245–256
NUCLEAR INSTRUMENTS & METHODS IN PHYSICS RESEARCH Section A
www.elsevier.com/locate/nima

Position-sensitive Si pad detectors for electron emission channeling experiments

U. Wahl[a,b,*], J.G. Correia[a,b,c], A. Czermak[d], S.G. Jahn[e], P. Jalocha[d], J.G. Marques[a,b], A. Rudge[c], F. Schopper[f], J.C. Soares[b], A. Vantomme[g], P. Weilhammer[c], the ISOLDE collaboration[c]

[a] *Instituto Tecnológico e Nuclear, Estrada Nacional 10, PT-2686-953 Sacavém, Portugal*
[b] *Centro de Física Nuclear de Universidade de Lisboa, PT-1649-003 Lisboa, Portugal*
[c] *CERN-EP, CH-1211 23 Genève, Switzerland*
[d] *Institute of Nuclear Physics, PL-31-342 Krakow, Poland*
[e] *Paul Scherrer Institut, CH-5232 Villigen, Switzerland*
[f] *Max-Planck-Institut für Extraterrestische Physik, D-85740 Garching, Germany*
[g] *Instituut voor Kern- en Stralingsfysica, Katholieke Universiteit Leuven, Celestijnenlaan 200 D, B-3001 Leuven, Belgium*

Received 4 November 2003; accepted 10 December 2003

Abstract

Position-sensitive detector systems, initially developed for the detection of X-rays, have been adapted for their use in electron emission channeling experiments. Each detection system consists of a $30.8 \times 30.8\,mm^2$ 22×22-pad Si detector, either of 0.3, 0.5 or 1 mm thickness, four 128-channel preamplifier chips, a backplane trigger circuit, a sampling analog to digital converter, a digital signal processor, and a personal computer for data display and storage. The operational principle of these detection systems is described, and characteristic features such as energy and position resolution and maximum count rate, which have been determined from tests with conversion electrons and β^- particles in the energy range 40–600 keV, are presented.

PACS: 07.77.−n; 07.77.Ka; 61.72.−y

Keywords: Position-sensitive detectors; Si pad detectors; Electron detection; Emission channeling; Lattice location

1. Introduction

Position-sensitive semiconductor detectors for minimum ionizing particles have originally been pioneered by high-energy physics applications [1,2], but have meanwhile found more and more applications, e.g. in astronomy [3], medical imaging [4] or chemical and biological structure analysis [5]. While most of the applications outside high-energy physics focus on X-ray detection, position-sensitive detectors (PSDs) for electrons are found scarcer. In this paper, we report on PSD systems adapted to lattice location studies of

*Corresponding author. Instituto Tecnológico e Nuclear, Estrada Nacional 10, Sacavém PT-2686-953, Portugal. Tel.: +351-2199-46085; fax: +351-2199-41525.
E-mail address: uwahl@itn.mces.pt (U. Wahl).

0168-9002/$ - see front matter © 2004 Elsevier B.V. All rights reserved.
doi:10.1016/j.nima.2003.12.044

radioactive atoms in single crystals by means of the electron emission channeling technique, an application in nuclear solid state physics. The emission channeling method [6,7] is based on the fact that charged particles from nuclear decay (α, β^-, β^+, conversion electrons) experience channeling or blocking effects along major crystallographic axes and planes. The resulting anisotropic emission yield from the crystal surface characterizes the lattice site occupied by the probe atoms during decay. The sensitivity of emission channeling with respect to the required number of probe atoms can be up to 4 orders of magnitude higher than in conventional lattice location experiments using the channeling of ion beams [8]. Hence emission channeling is especially suited in order to study systems where conventional ion beam techniques cannot be applied due to a lack of sensitivity, and has found various applications in materials science.

The simplest experimental approach to emission channeling is to rotate the single-crystalline sample in front of a collimated particle detector by means of a goniometer, and measure the angular-dependent count rate step by step. Using this technique, a variety of lattice location experiments in metals and semiconductors have been carried out throughout the last 15 years [6,7]. However, emission channeling is more conveniently measured using PSDs with larger solid angles, which increases the detection efficiency by about two orders of magnitude. Additional advantages are that there is no need for high-precision computer-controlled goniometers, and that it is not required to normalize the counting time per angular position to the sample activity. In the case of MeV alpha particles, suitable PSD systems were developed already in the 1970s, applying the principle of resistive charge division (see, e.g., Refs. [2,9]), and they are commercially available from several suppliers. The use of PSDs to detect MeV α emission channeling has already been reported in the literature [10–12]. However, α-emitting isotopes mainly exist, with a few exceptions, at masses above ≈ 150. On the other hand, β^-, β^+ or conversion electron emitters can be found for most elements of the periodic system, which makes position-sensitive detection of these particles very attractive. The PSD system described below has originally been developed [13] for X-ray applications in a Compton camera [14], but, with some modifications, turned out to be well adapted for electron measurements, and has been successfully used for conversion electrons of energies 40–250 keV and β^- particles up to 600 keV [15–22].

2. Requirements for PSDs for electron emission channeling

Conversion electrons are emitted from excited nuclear states and have discrete energies, typically of the order of 30–300 keV. In order to discriminate contributions from different isotopes or nuclear states and to subtract the background due to backscattered electrons, an energy resolution better than 10 keV is highly desirable for conversion electron experiments. For β^- and β^+ particles, which have continuous spectra with end point energies in the range of several hundred keV to several MeV, background correction is not feasible anyhow and a worse energy resolution can be tolerated.

An important characteristic in channeling experiments is the relative angular resolution $\Delta\theta/\theta$. Using a PSD it is limited by both the position resolution σ_d of the detector and the resolution σ_b due to the size of the radioactive spot on the sample. The latter is referred to as "beam spot" since emission channeling samples are usually produced by ion implantation. Approximately,

$$\Delta\theta/\theta \approx \Delta\theta d/s \approx 1/d(\sigma_d^2+\sigma_b^2)^{1/2} d/s \approx (\sigma_d^2+\sigma_b^2)^{1/2}/s \quad (1)$$

where θ is the opening angle of the detector with respect to the sample, which is approximately given by s/d, where s is the linear dimension of the detector and d the distance towards the sample. A natural limit to the detector's position resolution σ_d is the lateral straggling of the electrons in the detector itself. Its magnitude is comparable to the thickness required to completely stop all electrons, which in Si is around 7 μm at 30 keV, 350 μm at 300 keV, 900 μm at 600 keV, and 2 mm at 1 MeV

[23]. The beam spot resolution, σ_b, on the other hand, is usually limited by the fact that samples are produced by ion implantation of radioactive isotopes where beam spots much smaller than 1 mm are difficult to achieve. If a relative angular resolution better than, say, 10% is required, it is easily derived from the above equation that this demands for detectors with at least cm dimensions and mm or better position resolutions.

An additional requirement for electron PSDs is an entrance window which is sufficiently thin (less than a few μm) to let the electrons penetrate into the detector without excessive energy loss and straggling. Many PSDs that are optimized for X-rays do not meet this demand. Finally it should be taken into account that electron detectors have to be operated in vacuum. Unless actively cooling the device this puts limits on the tolerable heat generation within the detector and the readout electronics in its proximity.

While Si drift detectors [24] or Si charged coupled devices (CCDs) for nuclear applications [24–26] are also well suited for the position-sensitive detection of conversion electrons, as has been demonstrated recently [27], existing prototypes are still rather expensive. Note that multichannel plates, which are frequently applied as PSDs for X-rays or keV ions [3], are not suited due to their complete lack of energy resolution.

3. Layout of the detector and readout electronics

3.1. Detector design

The Si pad sensors [13] have been fabricated by the Swiss Center for Electronics and Microtechniques CSEM[1] and by the Norwegian company SINTEF.[2] The sensors have a square shape with $30.8 \times 30.8\,mm^2$ sensitive area and 484 pads. Single pads ($1.4 \times 1.4\,mm^2$) are defined by photolithography. The wafers are n-type material with a resistivity of 5 kΩ cm. Boron implantation (60 keV) is performed through a 500 Å thick implantation oxide with a dose of $5 \times 10^{14}\,cm^{-2}$. The gap between implanted pads is 40 μm. The ohmic back side of the sensor is prepared in such a way that the entrance window for electrons, defined by the n^+ implant depth and the thickness of the Al contact, is rather shallow to minimise charge loss in these layers. The backside of the sensor is implanted with phosphorus at 60 keV through a 500 Å thick implantation oxide at a dose of $3 \times 10^{15}\,cm^{-2}$. Simulation of this implantation process gives a profile with the n^+-doping concentration falling off from about $3 \times 10^{20}\,cm^{-3}$ to zero at a depth of about 3000 Å.

Metal contacts in metal layer 1 on top of the p^+ implant area are implemented by sputtering of Al with a thickness of 0.5 μm. A thick oxide (~5 μm) is formed on top of the metal 1 layer. After etching vias through the thick inter-metal oxide insulator, a 3 μm thick Al layer is sputtered on top of the thick oxide (metal 2). This metal layer serves to make ohmic contact to the metal 1 pads. By photolithography a narrow line pattern, with line width of 7 μm, is defined on the metal 2 layer. These lines connect the p^+ implants to the bond pad arrays arranged on the four sides of the detector. The 128 bond pads have a size of $60 \times 120\,\mu m^2$ each, with a transverse distance of 50 μm, and are arranged in two rows. These bond pad arrays match the bond pads on the readout chips. The p^+ pad area is surrounded by a p^+ guard ring. An oxide passivation layer of 2 μm thickness is applied to the pad side of the sensor. The area above the bond pads is opened by photolithography and etching. After removing the intermediate oxide protection layer the n^+ side is covered with a 500 Å thick Al layer by evaporation. The Al layer is sintered at 420°C for 60 min in N_2/H_2 gas mixture.

3.2. Readout electronics

The detection systems are equipped with four VA 1 readout chips[3] which are further developments of the VIKING chips [28–30] and are

[1] Centre Suisse d' Electronique et de Microtechnique SA, Jaquet-Droz 1, CH-2007 Neuchatel, Switzerland.

[2] SINTEF Electronics and Cybernetics, P.O. Box 124, N-0314 Oslo, Norway.

[3] A VLSI chip produced by Integrated Detector &Electronics AS (IDEAS), Gaustadalléen 21, N-0371 Oslo, Norway.

similar to the VA 3 chips described in Ref. [31]. Among the family of VA chips we have chosen for the VA 1 type because this chip offers for our detectors the best compromise between dynamic range (± 10 MIPS) and average noise ($\approx 170e^- + 7e^-/pF$). Each chip consists of 128 preamplifier channels with multiplexed readout electronics realized in 1.2 μm metal-oxide semiconductor very large-scale integrated (CMOS VLSI) technology and is connected to 121 pads on one of the four edges of the Si pad detector as shown in Fig. 1. The detector and the four VA readout chips are mounted on a hybrid with a 50-pin connector to the external signal and power lines. The n^+ backplane electrode of the detector is connected to a charge sensitive amplifier which employs a high transconductance input field effect transistor (FET) to match the high capacitance of the sensor backplane [13]. The discriminated output of this amplifier drives the backplane trigger electronics. For the use in channeling experiments the whole hybrid, including detector, VA readout chips and the backplane preamplifier circuit, is mounted within a high-vacuum chamber ($<10^{-6}$ mbar) and connected to the external electronics and power supplies by electrical vacuum feedthroughs. A simplified block diagram of the detector and readout chain is presented in Fig. 2, and the timing of the readout sequence in Fig. 3.

Within the VA chips, each channel has its own preamplifier, shaper and sample/hold circuit. If the backplane pulse amplitude exceeds the threshold voltage of an externally set lower level discrimi-

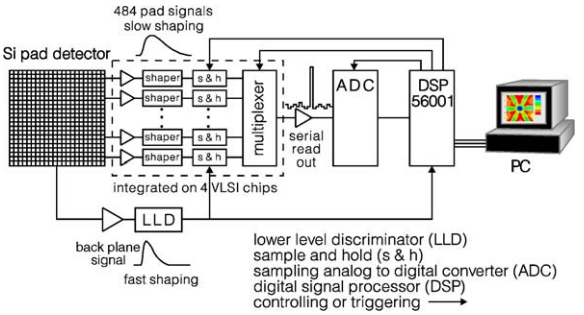

Fig. 2. Simplified block diagram of the detector and readout chain, from Ref. [18].

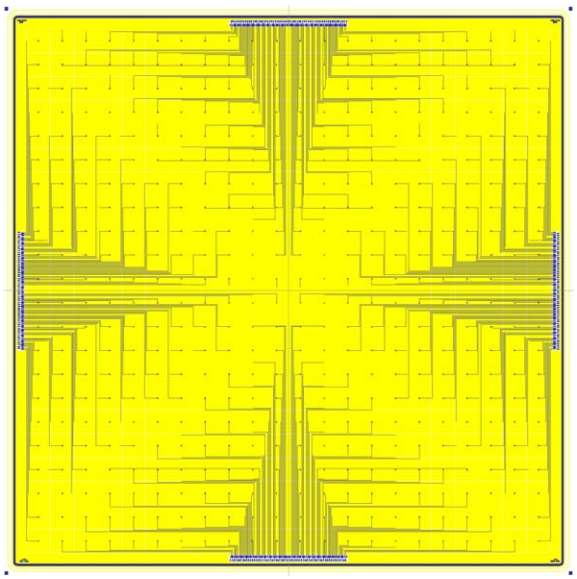

Fig. 1. Layout of the detector front side, showing the Al contacts leading to the 484 pads, from Ref. [13].

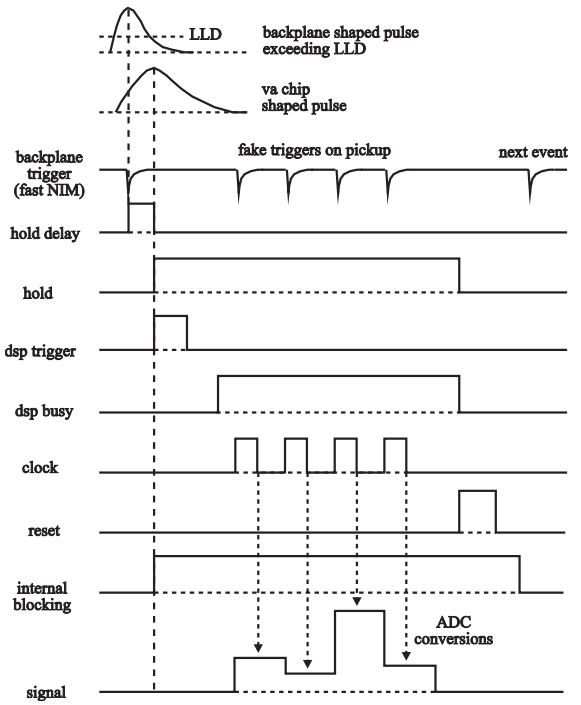

Fig. 3. Detector readout sequence in simplified form (only one chip with four channels shown).

nator, which is realized as a zero-crossing peak finding nuclear instrument module, the readout sequence is started in a digital signal processor (DSP). As DSP we use a Motorola 56001, programmed in assembler language. After a delay which corresponds to the picking time of the VA chips (1.5–2 μs) the DSP generates the hold signal which stores the analog information of each channel into its sample/hold circuit. At the same time the DSP sets internal and external blocking signals so as to prevent the system from accepting another trigger until the present readout cycle is completely finished. This procedure is also necessary in order to ignore fake backplane trigger pulses caused by pickup of the clock signals. The multiplexed readout of all channels is based on a Shift_in bit chained through all the chips, which during the readout cycle enables one of 512 channels to place its analog information on differential lines, one at any given clock pulse. With the first clock pulse sent to the first VA chip the DSP module sends the Shift_in bit which enables the first channel in the chain to be read out. The sampling analog to digital conversion of the DC signal that is delivered from the selected VA channel to the input of the ADC, takes place on the falling edge of the clock pulse. Following every A/D conversion, the digitized result is transferred to the DSP. The readout cycle for one event ends when the last of the 512 VA chip channels has been processed. In addition to controlling the overall timing, the DSP also performs the following analysis of the event during and immediately following the readout cycle:

1. The average DC offset of each VA channel, the so-called pedestal, is tracked and updated by a low pass filter with a time constant of 16 events. The pedestals are subtracted from the readout of every channel.
2. Following the subtraction of the pedestals, the DC offset common to all channels of the same chip, the so-called common mode, is calculated for this event. To remove the influence of noisy channels and of particle signals, the four channels with the largest (most positive) and the four channels with the smallest (most negative) output are excluded when determining the common mode. The common mode is then also subtracted from the readout of every channel.
3. Following subtraction of pedestals and common mode, the root mean square (rms) noise $\sigma_{\text{channel\_track}}$ is tracked for each chip channel separately and updated by a low pass filter with a time constant of 16 events.
4. The rms noise averaged over all the signals belonging to the same chip, $\sigma_{\text{chip\_event}}$, is computed for this event and its track value, $\sigma_{\text{chip\_track}}$, also updated by a low pass filter with a time constant of 16 events. Like for the common mode the four most positive and negative signals are excluded.
5. As a first selection threshold, the signal of every channel is compared to the chip noise $\sigma_{\text{chip\_event}}$ of this event. Only channels which are above the threshold $T_1\ \sigma_{\text{chip\_event}}$ (usually $T_1 = 3$ is chosen) are considered for output.
6. As second selection threshold, the signal height of these channels is compared to the corresponding channel noise and, if above $T_2\ \sigma_{\text{channel\_track}}$, it is finally marked for output.
7. All channels marked for output as well as those that are in direct neighbourhood are passed to the PC by means of direct memory access (DMA). The common modes and the average chip and channel noises, $\sigma_{\text{chip\_track}}$ and $\sigma_{\text{channel\_track}}$, are passed there, too.

On the PC a specially designed data acquisition and display program is running. Besides visualising energy and position spectra, and device parameters such as chip noises, channel noises, etc., the program allows to write event by event to the PC hard disk in list mode. For debugging and testing purposes, all the information transmitted from the DSP can be saved to disk. For the routine acquisition of channeling patterns, we found it in most cases sufficient, as will be shown below, to save only the signal with maximum amplitude and the address of the corresponding pad, requiring 9 Bytes per event.

4. Detector performance

Three types of detectors, with thickness of 0.3, 0.5 and 1 mm, were tested. The 0.3 and 0.5 mm thick devices could be fully depleted by applying bias voltages of 100 and 130 V, respectively. The pn junction being on the p^+ implanted front side of the detectors, these two detectors were used in the fully depleted state with the backside facing the sample. This configuration was preferred since the Al contact (500 Å) on the backside offers a thinner entrance window than the thick oxide (5 μm) that covers most of the pad side. In addition, the backside is less sensible to stray light and easier to clean from eventual dust. The 1 mm thick detector, on the other hand, could not be fully depleted without developing excessive noise, hence it had to be used with the pad side facing the sample.

4.1. Energy range and resolution

The output buffer of the VA1 chip saturates at ± 30 fC, which corresponds to an energy deposition of 680 keV in Si, and only electron energies up to approximately 400 keV can still be measured with linear response. The lower energy limit of detection, around 40 keV, is posed by the ability to discriminate low-pulse-height events from the relatively noisy backplane trigger signals. This is discussed in more detail in Section 4.3.

Each channel within the VA chips represents a separate amplifier with varying DC offset and gain. Channel to channel gain variations can be as high as 10% within a single chip. As was described above, the DC offset is removed already during data acquisition by means of pedestal subtraction. In order to define an integral energy resolution of the whole device, every channel must also be corrected for its gain. The gains are obtained by analyzing, separately for every pad, the energy spectrum of a single line gamma or electron source. The procedure is straightforward and has been described in detail earlier [13]. Following proper gain correction the contribution of gain variations to the integrated energy resolution is small. This can be seen by comparing the typical single pad resolution for the 59.537 keV gamma source ^{241}Am (Fig. 4(a)), which is around 3.0 keV full-width half-maximum (FWHM), to the integral energy resolution of the whole device for which we obtained 3.3 keV (Fig. 4(b)).

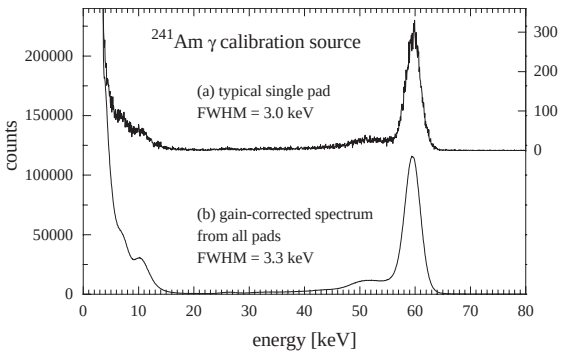

Fig. 4. Gamma energy resolution for a single pad (a) compared to the integrated energy resolution of the whole detector following gain-correction (b). The lower level threshold was set at 47 keV.

The energy resolution of each pad is influenced by the following factors: leakage current and capacity of the pad, electronic noise, time walk of the trigger, and effects due to incomplete energy deposition. For β particles in addition the energy loss and straggling in the detector entrance window must be taken into account. The contributions due to leakage current, capacity and electronic noise can be obtained from the rms value $\sigma_{\text{channel\_track}}$ of the noise calculated during data acquisition for the pads without hits. Typical rms noise levels per pad were $\sigma_{\text{channel\_track}} = 0.8-1.1$ keV. By using the relation FWHM = 2.35 rms, we conclude that this represents a contribution of 1.9–2.6 keV to the energy resolution and hence accounts for most of the photon energy resolution at 60 keV. The remaining difference we attribute mainly to the time walk between the backplane signal (which triggers the hold procedure on the VA chips) and the actual charge collection process in the pads and preamplifier chips.

Incomplete energy deposition results either from processes where particles escape from the detector without depositing their full energy (e.g. backscattered electrons) or from events where the generated charge is shared between several pads. The backscattering of electrons is a common phenomenon in radiation detection [2] and the

fraction of electrons backscattered from Si is expected to be around 12–14% in the energy range 50–500 keV [32]. As a consequence of backscattering, the energy spectrum of a mono-energetic electron source shows an asymmetric "full energy" peak, which is broadened in comparison to the photon response, and a pronounced tail stretching to lower energies.

The influence of charge sharing events on the energy resolution was studied in more detail using the 150 and 199 keV conversion electrons from the isotope ^{167m}Er (Fig. 5). For these energies, on average 2.7 and 5.4 keV, which correspond to 1.9% and 2.8% of the total charge, were deposited outside the pad that received the highest charge. The degradation of the energy resolution due to the charge sharing, however, was found to be not very pronounced at these energies. A "maximum hit only" spectrum, i.e. a spectrum that considered only the signals from the pads that received the highest charge per event (the normal mode of operation), showed energy resolutions of 5.7 and 5.8 keV at 150 and 199 keV, respectively (Fig. 5(a)). On the other hand, an "isolated hit" spectrum, i.e. a spectrum where those events were rejected in which the charge on one or more pads directly neighbouring the pad with maximum charge was greater than the mean noise of the event, $\sigma_{\text{chip\_event}}$, showed only slightly improved energy resolutions of 5.4 and 5.6 keV (Fig. 5(b)). Since the charge that is lost on neighbouring pads increases with electron energy, charge-sharing events are also responsible for some non-linearity in the energy response. The effect of charge-sharing can be removed from the energy spectrum to a large extent by, instead of only considering the signal from the pad that received the highest charge, adding the charge from the eight surrounding pads (Fig. 5(c)). However, this procedure is subject to the noise in a total of nine pads and hence the energy resolution deteriorates considerably to 8.1 keV at 150 keV and 7.8 keV at 199 keV. In practice, the influence of charge sharing events on energy resolution and linearity does not represent a serious drawback for channeling measurements.

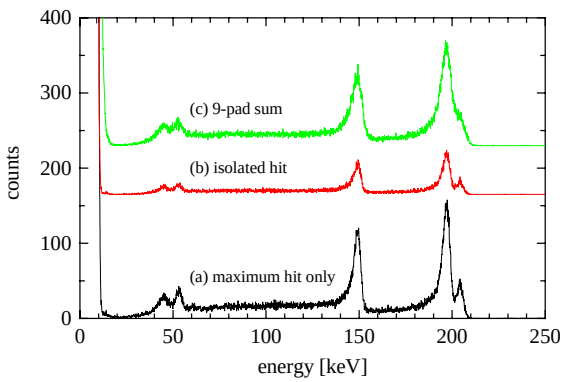

Fig. 5. Energy spectrum of ^{167}Tm recorded with the 0.3 mm thick detector, showing the conversion electron lines at 48.0, 55.9, 150.3, 198.9 and 206.0 keV. Spectrum (a) recorded only the signal from the pads that received the highest charge (normal mode of operation), (b) shows a spectrum where charge-sharing events were rejected, and (c) a spectrum where the charge sum from 9 pads was considered. Note that spectrum (a) and (b) have been shifted vertically for clarity.

The energy loss of electrons in the detector entrance windows depends on the configuration in which the detectors are used. In the configuration where the backside faces the sample, the entrance window consists of 500 Å of Al and up to 3000 Å of n^+-doped Si only. Using the energy calibration from the 59.537 keV gammas, a downward shift of 1.5 keV of the full energy peak of 63.6 keV electrons from ^{197m}Hg was observed. The contribution to the energy resolution from energy loss straggling in the entrance window is therefore negligible in this configuration (note that for higher electron energies the energy loss in the entrance window becomes even smaller). For detectors used with the pad side facing the sample, there are more pronounced effects. In this case the entrance window consists of 5 μm of SiO_2, 0.5 μm of Al and around 3000 Å of p^+ Si. Here, the observed shift in the full energy electron peak was 10.3 keV at 53.5 keV and 5.0 keV at 138.6 keV.

4.2. Position resolution

Apart from the shape and size of the pads, the position resolution of the detector is also influenced by the lateral straggling of the electrons leading to events where the charge is shared among several pads. This effect has been studied in more

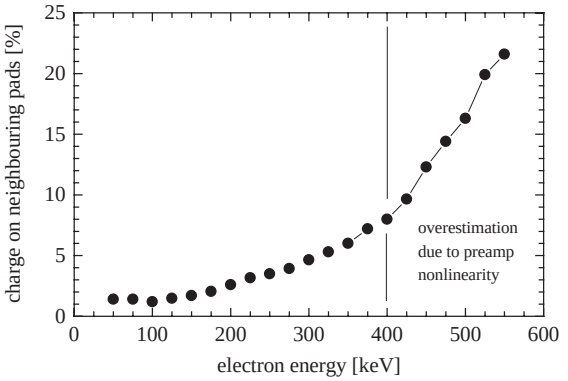

Fig. 6. Fraction of total charge deposited on pads neighbouring to the pad which received the highest charge. The electron energy was calculated from the charge sum of the events. Note that the fraction is overestimated above 400 keV due to the nonlinearity of the energy scale introduced by the gain saturation of the preamplifier chips.

detail (Fig. 6) using the continuous β^- spectrum of ^{67}Cu with electrons up to 577 keV energy. As can be seen, the fraction of charge deposited on neighbouring pads is less than 5% up to 300 keV, less than 8% up to 400 keV, but rises quite sharply at higher energies. For the typical low to medium energy β^- emitting isotopes in the emission channeling studies, however, this does not represent a serious problem since only a small fraction of betas receive energies in excess of 300 keV, e.g. for ^{67}Cu only 8%, for ^{59}Fe (461 keV endpoint energy) 4.9%.

As a simple maximum likelihood approach, we have chosen to consider the pad which received the highest charge as the point of electron impact, which avoids checking for multiple hits. In order to achieve maximum position resolution one could in principle identify the charge sharing events and exclude them from the data analysis or even data acquisition. However, this would either require saving all information from every event on disk in order to do an off-line analysis, or to implement the analysis procedure in the DSP program. While the former would require storing hundreds of Megabytes instead of a few MB per channeling pattern, the latter would decrease the maximum count rate considerably.

4.3. Maximum count rate

The characteristic feature limiting the count rate of the detection system is the backplane trigger technique which requires to read out all 512 chip channels per event and to process all the data by the DSP in order to locate the particle impact. We used an ADC capable of a maximum sampling rate of 1 MHz, which allowed setting the processing time for consecutive conversions to 1.2 μs. The algorithm of the DSP program for the on-line data analysis and selection was optimised so as to take advantage of the 1.2 μs processing time during which the ADC is busy. For the readout of 512 channels, the selection and the transfer of meaningful data to a PC, the DSP needs on average about 2 ms, so the entire count rate can reach at maximum 400–500 Hz. In practice, due to the random nature of the incoming particles, saturation was achieved around 250 events/s. This is sufficient, however, for typical emission channeling experiments using long-lived radioactive isotopes with half-lives of several hours and above.

As was already mentioned, the backplane triggering technique also severely limits the detection efficiency at lower energies. This is due to the fact that the noise of the backplane signal is dominated by the capacity and leakage current of the whole detector. Hence it is not possible to trigger on signals with less than 35 keV energy without saturating the maximum count rate by noise and receiving less than 1% of real events.

It is aimed to overcome the two principle shortcomings of the backplane triggering technique, i.e. count rate limitations and low energy detection efficiency, by using completely self-triggering preamplifier chips [29,31]. These allow reading out only those pads which have actually received a signal. Not only should this increase the maximum count rate to around 20 kHz, it is also expected to lower the accessible energy range to 10–15 keV.

5. Channeling measurements

As has been mentioned above, samples for emission channeling experiments are usually produced by

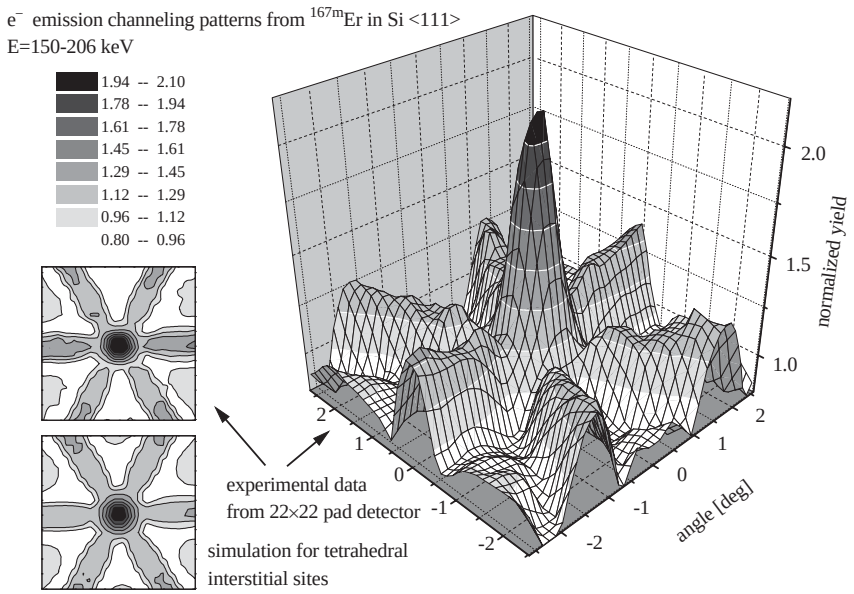

Fig. 7. ⟨1 1 1⟩ emission channeling pattern from the conversion electron emitter ^{167m}Er in Si. From this data together with the ⟨1 1 0⟩ pattern (not shown) it was concluded that Er is incorporated on near-tetrahedral sites in Si [15].

ion implantation into single crystals. In our case we use CERN's on-line isotope separator facility ISOLDE [33] for that purpose. ISOLDE provides a wide variety of radioactive isotopes as mass-separated 60 keV ion beams. However, the beams are only focused to a few mm, and spots of 1 mm diameter can usually only be achieved with a loss of 60–70% on a collimator in front of the sample. Therefore, while the detection efficiency of our pad system is 484 times higher than in conventional experiments not using position-sensitive detection, the overall experimental efficiency (including both isotope collection and measurement) is only roughly 150 times higher. This is due to the fact that conventional detection techniques can work with larger beam spots without loss of angular resolution, and hence do not require collimating the beam during implantation.

For typical electron channeling experiments an angular range of $6^\circ \times 6^\circ$ is sufficient, which allows to analyze the angle-dependent emission yield within $\pm 3^\circ$ in two dimensions around a channeling axis. With respect to the pad detector size of $s = 30$ mm, a distance of $d = 285$ mm between sample and detector has been chosen. Taking into account that the root mean square, σ, of a constant probability distribution of width w is given by $\sigma = 0.289w$, we derive rms position resolutions of $\sigma_d = 0.38$ mm due to the 1.4 mm size of the pads, and $\sigma_b = 0.29$ mm due to the size of the beam spot. Using Eq. (1), we therefore arrive at an overall angular resolution of $\Delta\theta = 0.095^\circ$, which allows to resolve typical electron channeling patterns, where the width of axial and planar effects is around 1–2°. Figs. 7 and 8 show as two examples the ⟨1 1 1⟩ channeling patterns resulting from the radioactive isotopes ^{167m}Er and ^{67}Cu in Si. In the case of the isotope ^{167m}Er, the pattern results from the sum of the conversion electrons at 150, 199 and 206 keV, in the case of ^{67}Cu, from the integral β^- intensity in the range 97–577 keV.

In order to clearly identify the lattice positions occupied by the probe atoms and to derive quantitative information on site fractions, the experimental patterns are compared to theoretical yields for a variety of different lattice sites by means of a fitting procedure. For that purpose, computer simulations of the angular emission yields of electrons are carried out. The concept of electron emission channeling simulations is based on the dynamical theory of electron diffraction and is described in detail in Refs. [6,7]. The

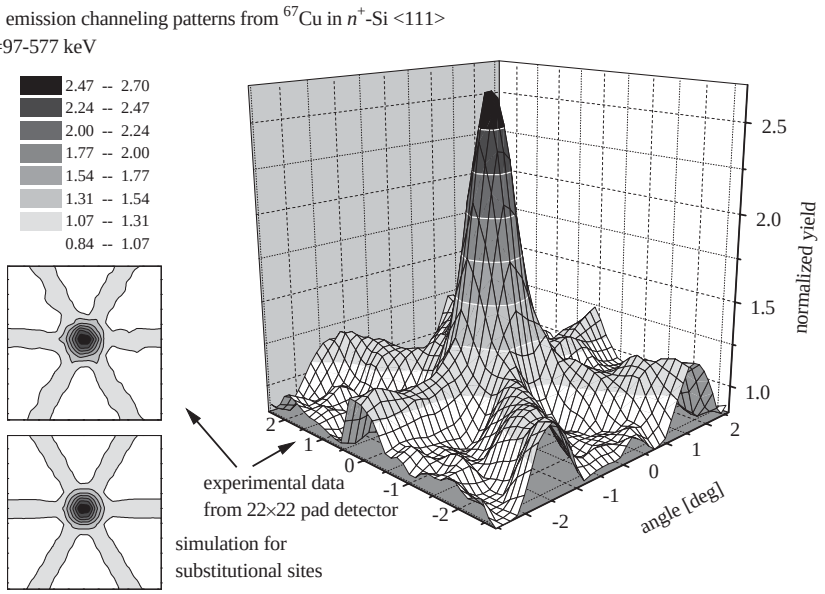

Fig. 8. ⟨1 1 1⟩ emission channeling pattern from the β^- emitter ^{67}Cu in n$^+$-Si, incorporated on substitutional sites.

simulations result in site-characteristic two-dimensional patterns of electron emission probability, $\chi_{\text{theo}}(\theta,\phi)$, where θ and ϕ denote polar and azimuthal angles from the axis. These patterns are smoothed using a Gaussian of $\sigma = 0.06^\circ$ to account for that part of the experimental angular resolution which is due to the 1 mm beam spot on the sample. The size and shape of the detector pads, however, is taken into account during fitting by averaging over the simulated yield falling within the angular range ($0.26^\circ \times 0.26^\circ$) of one pad. Theoretical emission patterns are fitted to the experimental yields, χ_{ex}, according to

$$\chi_{\text{ex}}(\theta,\phi) = S[f_1\chi_{\text{theo},1}(\theta,\phi) + f_2\chi_{\text{theo},2}(\theta,\phi) + f_3\chi_{\text{theo},3}(\theta,\phi) + 1 - f_1 - f_2 - f_3] \quad (2)$$

where S is a scaling factor common to all angles in one pattern, and f_1, f_2 and f_3 denote the fractions of emitter atoms on up to three different lattice sites. The random fraction, $f_R = 1 - (f_1 + f_2 + f_3)$, accounts for emitter atoms which cause negligible anisotropies in emission yield, i.e. which are located in sites of very low crystal symmetry or in heavily damaged or amorphous surroundings. In principle up to seven fit parameters, S, f_1, f_2, f_3, x_0, y_0 and ϕ_0, may be simultaneously optimized using non-linear least-square fitting routines. While the parameters S, x_0, y_0 and ϕ_0 are always allowed to vary in order to provide correct normalization of the experimental spectra and to achieve optimum translational and azimuthal orientation with respect to the detector, usually only one or two different site fractions, f_1 and f_2, are considered.

Three detection systems are in routine use for emission channeling experiments at CERN's ISOLDE facility. The majority of experiments focuses on the lattice location of implanted rare earth (e.g. ^{143}Pr, ^{167}Tm, ^{169}Yb) and transition metal (^{59}Fe, ^{67}Cu, ^{111}Ag) probe atoms in semiconductors such as Si, Ge, diamond, SiC, GaAs, InP, GaN, AlN and ZnO. These systems are of considerable technological interest. Rare earth atoms have a great potential as optical dopants [34–36]. Emission channeling experiments using ^{167m}Er gave the first direct evidence that implanted Er occupies near-tetrahedral sites in Si [15] (Fig. 7). Transition metals represent widespread contaminants in Si processing, acting as deep centers which can cause the failure of devices [37–39]. In the III–V semiconductors, on the other hand, transition metals are beneficially used in order to convert

n- or p-type crystals to semi-insulating material [40]. By means of β^- emission channeling it could be unambiguously proven that implanted Cu occupies near-substitutional sites in Si [17,19], which represents the first detailed lattice location experiment of Cu in a semiconductor. A further project is the study of High-T_c superconductors and related oxide materials. It is known that doping with Hg can raise the critical temperature for superconductivity, T_c, of $YBa_2Cu_3O_{6+x}$ by up to 10 K [41]. Combined emission channeling and perturbed angular correlation (PAC) experiments have shown that the radioactive isotope ^{197m}Hg is incorporated on the so-called Cu(1) sites in $YBa_2Cu_3O_{6+x}$ [42].

Up to now, the detection systems have been applied successfully in emission channeling experiments using the following isotopes: ^{24}Na, ^{45}Ca, ^{59}Fe, ^{67}Cu, ^{67}Ga, ^{73}As, ^{73}Se, ^{86}Rb, ^{89}Sr, ^{107}Cd, ^{109}Cd, ^{115}Cd, ^{111}Ag, ^{111}In, ^{121}Sn, ^{139}Ce, ^{141}Ce, ^{143}Pr, ^{147}Nd, ^{149}Pm, ^{149}Gd, ^{153}Sm, ^{155}Eu, ^{155}Tb, ^{167}Tm, ^{169}Yb, ^{170}Lu, ^{181}Hf, ^{195m}Hg, ^{197m}Hg, and ^{203}Hg. Even in the case of the medium energy β^- emitting isotopes ^{24}Na (endpoint energy 1389 keV), ^{111}Ag (1035 keV), ^{143}Pr (935 keV) and ^{89}Sr (1495 keV) it was found that the detectors responded with sufficient position resolution for lattice location measurements.

6. Conclusions

While the pad detectors were initially developed for X-ray applications, our successful tests and channeling measurements show that they are also very suitable for the position-sensitive detection of electrons. The presented devices represent a great advance in measuring electron emission channeling effects from isotopes with half-lives longer than a few hours, increasing the overall experimental efficiency by roughly two orders of magnitude. The detection systems have already found wide applications for lattice location experiments in semiconductors, oxides, and high-T_c superconductors. In the future, we expect to improve the lower limit of the accessible energy range, the trigger efficiency at low energies and the maximum count rate by using completely self-triggering readout chips.

Acknowledgements

This work was funded by the Foundation for Science and Technology, Portugal (FCT, project CERN/FIS/43725/2001) and partly by the European Union (Large Scale Facility contract HPRI-CT-1999-00018). U. Wahl acknowledges his fellowship supported by the FCT.

References

[1] G. Hall, Rep. Prog. Phys. 57 (1994) 481.
[2] G.F. Knoll, Radiation Detection and Measurement, Wiley, New York, 2000.
[3] J.L. Culhane, Nucl. Instr. and Meth. A 310 (1991) 1.
[4] R.J. Ott, Nucl. Instr. and Meth. A 392 (1997) 396.
[5] A.R. Faruqui, Nucl. Instr. and Meth. A 310 (1991) 14.
[6] H. Hofsäss, G. Lindner, Phys. Rep. 201 (1991) 123.
[7] H. Hofsäss, Hyperfine Interactions 97 (1996) 247.
[8] L.C. Feldman, J.W. Mayer, S.T. Picraux, Materials Analysis by Ion Channeling, Academic Press, New York, 1982.
[9] E. Lægsgaard, Nucl. Instr. and Meth. A 162 (1979) 93.
[10] U. Wahl, H. Hofsäss, S.G. Jahn, S. Winter, E. Recknagel, The ISOLDE collaboration, Nucl. Instr. and Meth. B 64 (1992) 221.
[11] M. Lindroos, H. Haas, J. De Wachter, H. Pattyn, G. Langouche, Nucl. Instr. and Meth. B 64 (1992) 256.
[12] U. Wahl, Phys. Rep. 280 (1997) 145.
[13] P. Weilhammer, E. Nygård, W. Dulinski, A. Czermak, F. Djama, S. Gadomski, S. Roe, A. Rudge, F. Schopper, J. Strobel, Nucl. Instr. and Meth. A 383 (1996) 89.
[14] J.W. LeBlanc, N.H. Clinthorne, C.H. Hua, E. Nygård, W.L. Rogers, D.K. Wehe, P. Weilhammer, S.J. Wildermann, IEEE Trans. Nucl. Sci. NS-45 (1998) 943.
[15] U. Wahl, A. Vantomme, J. De Wachter, R. Moons, G. Langouche, J.G. Marques, J.G. Correia, The ISOLDE collaboration, Phys. Rev. Lett. 79 (1997) 2069.
[16] U. Wahl, J.G. Correia, S. Cardoso, J.G. Marques, A. Vantomme, G. Langouche, The ISOLDE collaboration, Nucl. Instr. and Meth. B 136 (1998) 744.
[17] U. Wahl, A. Vantomme, G. Langouche, J.G. Correia, The ISOLDE collaboration, Phys. Rev. Lett. 84 (2000) 1495.
[18] U. Wahl, Hyperfine Interactions 129 (2000) 349.
[19] U. Wahl, A. Vantomme, G. Langouche, J.P. Araújo, L. Peralta, J.G. Correia, The ISOLDE collaboration, Appl. Phys. Lett. 77 (2000) 2142.

[20] U. Wahl, A. Vantomme, G. Langouche, J.P. Araújo, L. Peralta, J.G. Correia, the ISOLDE collaboration, J. Appl. Phys. 88 (2000) 1319.
[21] U. Wahl, A. Vantomme, G. Langouche, J.G. Correia, L. Peralta, the ISOLDE collaboration, Appl. Phys. Lett. 78 (2001) 3217.
[22] U. Wahl, E. Rita, E. Alves, J.G. Correia, J.P. Araújo, the ISOLDE collaboration, Appl. Phys. Lett. 82 (2003) 1173.
[23] G. Bertolini, A. Coche (Eds.), Semiconductor Detectors, North-Holland, Amsterdam, 1968.
[24] J. Kemmer, G. Lutz, Nucl. Instr. and Meth. A 253 (1987) 365.
[25] C.J.S. Damerell, Rev. Sci. Instr. 69 (1998) 1549.
[26] L. Strüder, Nucl. Instr. and Meth. A 454 (2000) 73.
[27] H. Hofsäss, U. Vetter, C. Ronning, M. Uhrmacher, K. Bharuth-Ram, R. Hartmann, L. Strüder, Nucl. Instr. and Meth. A 512 (2003) 378.
[28] E. Nygård, P. Aspell, P. Jarron, P. Weilhammer, P. Yashioka, Nucl. Instr. and Meth. A 301 (1991) 506.
[29] P. Aspell, R. Boulter, A. Czermak, P. Jalocha, P. Jarron, A. Kjensmo, W. Lange, E. Nygård, A. Rudge, O. Toker, M. Turala, H. Von Der Lippe, U. Walz, P. Weilhammer, K. Yoshioka, Nucl. Instr. and Meth. A 315 (1992) 425.
[30] O. Toker, S. Masciocchi, E. Nygård, A. Rudge, P. Weilhammer, Nucl. Instr. and Meth. A 340 (1994) 572.
[31] P. Weilhammer, Nucl. Instr. and Meth. A 497 (2003) 210.
[32] T. Tabata, R. Ito, S. Okabe, Nucl. Instr.and Meth. A 94 (1971) 509.
[33] E. Kugler, D. Fiander, B. Jonson, H. Haas, A. Przewloka, H.L. Ravn, D.J. Simon, K. Zimmer, the ISOLDE collaboration, Nucl. Instr. and Meth. B 70 (1992) 41.
[34] S.S. Iyer, Y.H. Xie, Science 260 (1993) 40.
[35] A. Polman, J. Appl. Phys. 82 (1997) 1.
[36] A.J. Steckl, J.M. Zavada, MRS Bull. 24 (9) (1999) 33.
[37] K. Graff, Metal Impurities in Silicon-Device Fabrication, Springer, Berlin, 1995.
[38] A.A. Istratov, E.R. Weber, Appl. Phys. A 66 (1998) 123.
[39] A.A. Istratov, E.R. Weber, Appl. Phys. A 69 (1999) 13.
[40] A. Gasparotto, A. Carnera, C. Frigeri, F. Priolo, B. Fraboni, A. Camporese, G. Rossetto, J. Appl. Phys. 85 (1999) 753.
[41] A.K. Chakraborty, K. Bose, G. Som, B.K. Chaudhuri, J. Mater. Sci: Mater. Electron. 5 (1994) 22.
[42] J.P. Araújo, J.G. Correia, U. Wahl, J.G. Marques, E. Alves, V.S. Amaral, A.A. Louren¸co, V. Galindo, T. von Papen, J.P. Senateur, F. Weiss, A. Vantomme, G. Langouche, A.A. Melo, M.F. da Silva, J.C. Soares, J.B. Sousa, the ISOLDE collaboration, Nucl. Instr. and Meth. B 147 (1999) 244.